

# Watermark Retrieval from 3D Printed Objects via Convolutional Neural Networks

Xin Zhang, Qian Wang, Toby Breckon and Ioannis Ivrissimtzis

Durham University

Department of Computer Science

Durham, DH1 3LE, UK

{xin.zhang3, qian.wang, toby.breckon, ioannis.ivrissimtzis}@durham.ac.uk

## Abstract

We present a method for reading digital data embedded in planar 3D printed surfaces. The data are organised in binary arrays and embedded as surface textures in a way inspired by QR codes. At the core of the retrieval method lies a Convolutional Neural Network, outputting a confidence map of the location of the surface textures encoding value 1 bits. Subsequently, the bit array is retrieved through a series of simple image processing and statistical operations applied on the confidence map. Extensive experimentation with images captured from various camera views, under various illumination conditions and from objects printed with various material colours, shows that the proposed method generalizes well and achieves the level of accuracy required in practical applications.

## 1 Introduction

*Additive manufacturing*, most commonly known as *3D printing*, is a manufacturing method that creates objects by adding one layer of material on top of the other. One of the advantages of additive manufacturing over more traditional methods is that it can handle geometries which either were impossible to manufacture, or the cost of their manufacturing was prohibitive [1].

*Watermarking*, a term used in a broad sense in this paper, is the embedding of information on a physical object or a digital file. It may serve various purposes, such as object or file authentication, copy control, protection against unauthorized alteration, or dissemination of machine readable information. The latter is an increasingly popular application, especially in the form of QR codes, and is the target application of the proposed method for watermarking 3D printed objects.

In this paper, aiming at exploiting the capability of 3D printing to create objects of more complex geometry at no additional cost, we propose a 3D surface watermark similar in design to QR codes. The information is embedded on the nodes of a regular grid, one bit per node, using semi-spherical or cubic bumps. The existence of a bump indicates a bit value of 1 at that node of the grid and its absence a bit value 0. See Figure 1 for some examples.

### 1.1 Motivation

We notice that the common practice of placing a printed QR code on or next to a physical objects is vulnerable to various malicious attacks. For example, an attacker could replace a printed QR code with their own, or overlay it, or in a phishing style attack put a printed QR code in a place where there shouldn't be one. The root cause of these vulnerabilities is that at the moment the



Figure 1: Examples of 3D printed surface watermarks.

manufacturing of an object and the embedding of information on it are two separate processes. 3D printing brings a unique opportunity to address the problem by integrating the information embedding process into the manufacturing process. That is, the embedded information can be part of the fabric of a 3D printed object, rather than been manufactured separately and glued on to it.

## 1.2 Challenges

The challenges in developing a 3D printing watermark method can be summarized as follows:

1. Since 3D printed objects are often created from a single material, the background surface and the watermark carrying bumps would often have the same colour and it would be difficult to distinguish between them.
2. The popularity of low-end printers with plastic filaments means that the carrier surface would often contain significant noise as well as various infill patterns created during slicing. For that reason, the sizes and shapes of the bumps may vary considerably, even if they are identical in the digital file. See Figure 2 (left).
3. Watermark retrieval is expected to be done from images captured by a hand-held phone camera under potentially adverse conditions. Apart from assuming an arbitrary camera viewpoint, the variability of the lighting conditions, which may range from smooth natural light to extremely uneven artificial illumination, should also be taken into account. See Figure 2 (middle and right).

Our experimental results show that convolutional neural networks can overcome this multitude of watermark retrieval challenges entailed into a realistic scenario.

## 1.3 Contributions

The main contributions of the paper are the development of a watermark retrieval algorithm the design and creation of an image database of 3D printed watermarked objects. The retrieval algorithm starts with a convolutional neural network generating an approximate density map representing the locations of watermark bumps in the input RGB image. The subsequent steps are a series of simple image processing and statistical operations. Specifically, the registration of the density map, a sequence of simple image processing operations, and finally, the retrieval of the watermark through the K-means clustering method. See Figure 3 for a high level description of the algorithm.

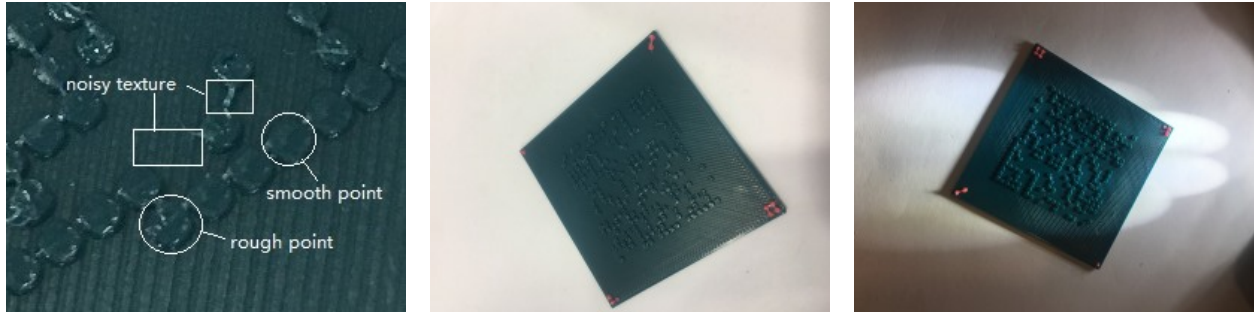


Figure 2: **Left:** Challenges related to the printing process. **Middle and Right:** Watermark retrieval challenges due to illumination: natural light (middle) and uneven artificial light (right).

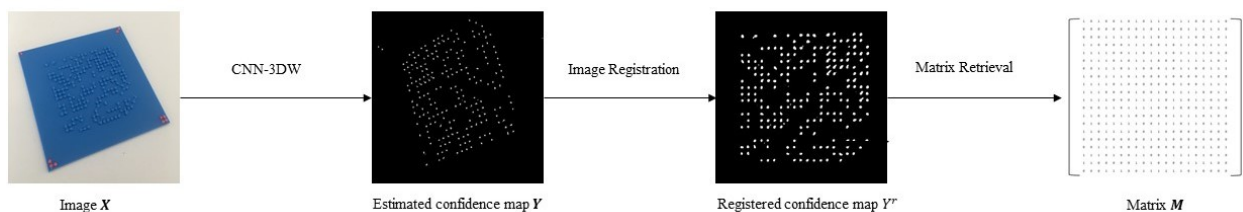


Figure 3: The pipeline of the proposed 3D watermarking retrieval method.

## 2 Related Work

Comprehensive reviews of additive manufacturing with academic or industrial focus can be found in [2, 3]. Currently, there is a multitude of competing additive manufacturing technologies, from laminated object manufacturing to photosensitive polymer curing molding to laser powder sintering molding. All our test objects were printed with fused deposition modeling, which is a low-cost and thus widely available 3D printing technology.

### 2.1 Digital 3D Watermarking

Digital 3D watermarking is an active, well-developed field [4, 5, 6, 7], mostly focusing on boundary surface representations of 3D models, triangle meshes in particular. The proposed watermarking of 3D printed surfaces has some obvious relationships with digital 3D watermarking. Indeed, the construction of a watermarked 3D printed object starts with the creation of a watermarked 3D file. However, the two processes diverge significantly during watermark retrieval. In digital 3D watermarking, we have to extract information from a digital file by inverting the embedding algorithm. In 3D printing watermarking in contrast, having to extract information from a physical object we are faced with a classic computer vision problem.

The challenge in the development of digital 3D watermarking algorithms is to make them robust against a variety of malicious or unintentional attacks, including 3D printing and rescanning. Watermark survivability under this attack has been tested in [8], while surface watermarking algorithms resilient to the attack have been proposed in [9]. Notice that the aim of the watermarking algorithm in [9] is to protect the digital 3D file from watermark removal attacks while here our aim to embed machine readable information on physical objects. Guided by different objectives, they restrict themselves to just 24 bits of payload and most importantly, retrieval involves 3D laser

scanning and surface reconstruction. In contrast, we do not make use of any specialized equipment such as laser scanners as we never reconstruct a digital 3D model from the 3D printed object.

## 2.2 Feature extraction

Convolutional neural networks have demonstrated impressive performance on a variety of computer vision tasks [10][11][12]. They are considered particularly well suited for feature extraction and classification tasks, AlexNet [13], VGGNet [14] and GoolgeNet [15] being some famous examples. Recently, deep CNN models have been employed for image based crowd counting tasks [16][17][18]. It is usually formulated as a regression problem with the raw images as input and outputting a feature map (i.e. density map) characterizing the density of crowd in the image. Here, following, we take the simple but effective approach of training a CNN to extract a confidence map.

In an earlier approach to the problem of 3D printed watermark retrieval we developed a technique for recognizing the watermark bumps based on local binary patterns (LBP) [19]. However, as it is often the case with hand-crafted feature extraction methods, the results did not generalize very well under adverse conditions, in particular when the background patterns were too prominent, or under extreme uneven illumination, or under unfavorable camera viewpoints.

## 3 Method

Given an image/photo of a printed watermark as shown in Figure 2, we aim to extract the information embedded in the watermark, which in our case is a binary matrix. To detect the surface bumps corresponding to bit value 1 we propose an image processing pipeline comprising of three stages (c.f. Figure 3). In the first stage, a fully convolutional network (FCN) takes an image  $\mathbf{X}$  as input and outputs an estimated confidence map  $\mathbf{Y} = f(\mathbf{X})$ . To overcome the issues of target scaling, rotation and affine distortion in the input images, in the second stage, image registration procedures are applied to the confidence map  $\mathbf{Y}$  to get a registered confidence map  $\mathbf{Y}^r$ . Finally, the information matrix  $\mathbf{M}$  is extracted from the registered confidence map  $\mathbf{Y}^r$ . In the following subsections, we explain these three stages in detail.

### 3.1 CNN-3DW

#### 3.1.1 Network Architecture

The proposed CNN based model for 3D watermark retrieval is a fully convolutional network named **CNN-3DW**. The architecture is shown in Figure 4. It consists of five convolutional layers in which there are 48, 96, 48, 24, 1 kernels with sizes of  $9 \times 9$ ,  $7 \times 7$ ,  $7 \times 7$ ,  $7 \times 7$ ,  $7 \times 7$  and  $1 \times 1$  respectively. The activation function is the Rectified Linear unit (ReLU), which generally performs well in CNNs, see for example [20]. Two max pooling layers with step size two are added after the first and second convolutional layers, respectively. For all the convolutional layers, we set the step size as one and do zero padding so that the image size is not altered by the convolution operations. As a result, the final output has one fourth the size of the input image due to two maxpooling layers. Since the whole network is fully convolutional, it is able to handle input images of different sizes.

#### 3.1.2 Ground Truth Confidence Map

Given an input image  $\mathbf{X}$  of a printed watermark, the goal of our CNN-3DW is to estimate the confidence map of ‘‘bump’’ locations representing the value of ones in the information matrix. Figure 5 shows an image of a watermarked object and its corresponding ground truth confidence

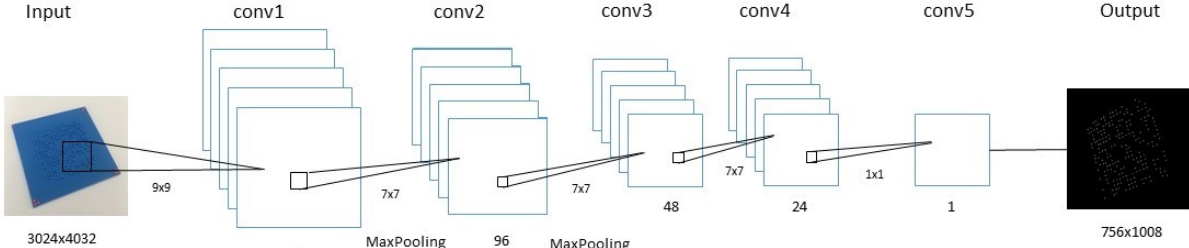


Figure 4: The architecture of the proposed CNN-3DW.

map and the estimated confidence map by the proposed CNN model. We need to annotate the training data for such purpose. Specifically, we generate the ground truth confidence map  $\mathbf{Y}$  based on the annotation image  $\mathbf{A}$  by a Gaussian smoothing process.

$$\mathbf{Y} = \mathbf{A} * \mathbf{G}_\sigma, \quad (1)$$

where  $*$  is a convolution operator applied on the binary annotation image  $\mathbf{A}$  and the Gaussian kernel  $\mathbf{G}_\sigma$ . The annotation image can be represented by

$$\mathbf{A}_{ij} = \begin{cases} 1 & \text{if } (i, j) \text{ is the centroid of a marked region,} \\ 0 & \text{otherwise.} \end{cases} \quad (2)$$

The annotation images are the results of human annotation on the training data while the standard deviation of Gaussian kernel was determined empirically to be  $\sigma = 5$ .

### 3.1.3 Model Training

To train the network, we use the mean squared error (MSE) loss function:

$$L(\Theta) = \frac{1}{N \times H \times W} \sum_{n,h,w} (f(\mathbf{X}; \Theta) - \mathbf{Y})^2, \quad (3)$$

where  $\Theta$  is the set of network parameters;  $N$  is the number of training images;  $\mathbf{X}$  is an input image,  $\mathbf{Y}_i$  the ground truth confidence map of  $\mathbf{X}$  and  $f(\mathbf{X}, \Theta)$  is the predicted confidence map of the input image  $X$ ;  $W$  and  $H$  are the width and height of the confidence map image  $\mathbf{Y}$  respectively.

Data augmentation techniques have proved to be beneficial to the training of deep CNN models, alleviating the overfitting issue especially in situations where the training data is not large enough. In our experiments we employ three data augmentation techniques to compensate for insufficient training data. Firstly, the images are randomly rotated by a random angle degrees. Secondly, the training data are augmented by randomly changing their average brightness. Finally, random cropping is applied to generate 10 patches of uniform size (i.e.  $512 \times 512$ ) from each image.

We trained the CNN-3DW with Keras [21] built on TensorFlow. The Adam optimizer [22], a stochastic gradient descent optimization method for training deep learning models, is employed with the default parameter values. We set the initial learning rate as  $1e - 5$  and decrease it to  $1e - 6$  after 50 epochs. The training is stopped after 100 epochs where we observed convergence of the model. When using an NVIDIA GeForce GTX TITAN X, the average training time was about 7 hours on our own dataset which will be introduced in the following section.

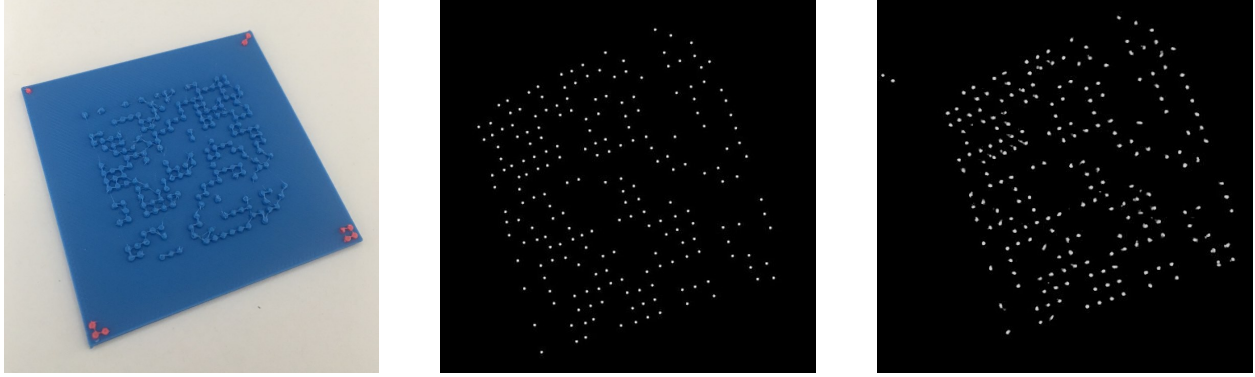


Figure 5: **Left:** image of a watermarked object. **Middle:** ground truth map. **Right:** corresponding confidence map.

### 3.2 Image registration, processing and matrix retrieval

Using the trained CNN-3DW model we are able to estimate a confidence map  $\mathbf{Y}$  of the watermark bumps in the image  $\mathbf{X}$ . To extract the embedded information matrix from the estimated confidence map  $\mathbf{Y}$  is still non-trivial. The first issue is that we need to locate the watermark regions in the confidence map. In our experiments, we observed that noises exist in the background regions of some images, posing great challenges to the automatic watermark region localization. Significant bias in the watermark region localization would lead to catastrophic error in the following stages. To fight this issue off, we print four *landmarks* at the corners of the watermark with easily distinguishable colours (see Figure 1). During retrieval, the watermark regions are easily located by finding the “differently coloured” *landmarks* at the four corners.

The second issue is that the watermark in the image could be of variant scales, rotations and affine distortions. To tackle this issue, we use image registration [23] to transform the watermark region in the confidence map  $\mathbf{Y}$  to a square region (see Figure 3). In image registration, the *landmarks* are used as control points which are supposed to be mapped to the four corners of the new square region. In our experiments, we used Matlab’s built-in tools for the image registration. After image registration, we obtain the transformed confidence map and the watermark region is cropped with the background region discarded. We denote the reserved watermark region of confidence map as  $\mathbf{Y}^r$ .

Finally, we extract the embedded information matrix  $\mathbf{M}$  from  $\mathbf{Y}^r$ . The registered confidence map  $\mathbf{Y}^r$  is firstly binarized by a threshold  $t$ ,

$$\hat{\mathbf{Y}}_{ij}^r = \begin{cases} 1 & \text{if } \mathbf{Y}_{ij}^r > t, \\ 0 & \text{otherwise.} \end{cases} \quad (4)$$

where  $t = \beta \times Thre$  and  $Thre$  is the OTSU threshold [24] of the registered confidence map  $\mathbf{Y}^r$ ,  $\beta$  is a user defined parameter. In our experiments we empirically set  $\beta = 0.35$  for optimised performance. The binary confidence map  $\hat{\mathbf{Y}}^r$  is visualized in Figure 6. We call Matlab’s *regionprops* function to detect the connected regions within the binary image and obtain estimates of their centroids and two semi-axes. If the the sum of the two semi-axes is above a threshold, a bit value 1 will be returned from the centroid of that region as shown in Figure 6. Now we end up with a set of coordinates representing the detected watermark bumps in  $\hat{\mathbf{Y}}^r$ . As a final step, we extract the information matrix  $\mathbf{M}$  from the set of coordinates. Ideally, there exist only  $m$  (the number of rows and columns of  $\mathbf{M}$ ) unique values for  $x$  and  $y$  coordinates, however, due to the imperfection of

the results of the previous steps, the coordinates have biases. To resolve this issue, we utilize a  $K$ -means clustering on the  $x$  and  $y$  coordinates of all the detected points, respectively. We set the number of clusters as  $m$  and rank the  $m$  cluster centers. The point falling into the  $i$ -th cluster will be assigned to a new coordinate in the  $m \times m$  matrix  $\mathbf{M}$ .

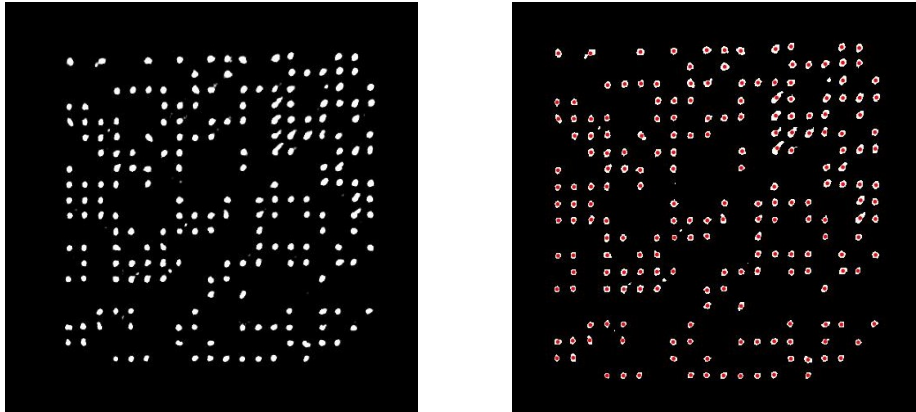


Figure 6: The regularised CNN-3DW output (left) and the detected centroids of bit value 1 regions (right).

## 4 Experiments

In this section, we conduct a series of experiments to evaluate the effectiveness of the proposed approach on 3D watermark retrieval. Since there are no datasets with images of 3D printed objects watermarked with a similar method, we designed our own dataset named **3DW-FS**<sup>1</sup>. We conduct five experiments and report the results in the following subsections.

### 4.1 Dataset: 3DW-FS

To collect a dataset as the test bed for our validation experiments, we first print watermarks on multiple objects, then collect images of the watermarked objects for our experiments. The watermarks printed on objects convey information encoded in  $20 \times 20$  binary matrices which are randomly generated and different for each object. The images are captured using a mobile phone camera which takes images of  $3024 \times 4032$  resolution. The dataset consists of 290 images from 20 objects printed with 9 different materials of different colour. We collect 15 images for each of the objects 1-16 and 5 images for each of objects 17-20. Figure 8 shows one exemplar image from each printed object. To simulate potential scenarios in practical applications, we captured images under variant conditions. Firstly, we collected 10 and 5 images under natural and extreme artificial illumination respectively for objects 1-16; while for objects 17-20, we collected 3 and 2 images under these two illumination conditional respectively. Secondly, we keep variant distances to the objects when collecting images, so that the watermark regions in the images have different sizes. Thirdly, we ensure that the watermarks in the collected images have variant rotations in both horizontal and vertical directions to expect that the watermark can be recognized from arbitrary perspectives. As a result, our dataset is challenging and provides a simulation of real scenarios.

<sup>1</sup>The whole dataset including raw images and the annotations will be made publicly available.



Figure 7: Exemplar images of objects 1-20 from left to right and top to down.

For the purpose of CNN model training, we manually annotate all the images of objects 1-16, i.e., 240 images in total. For the annotation, we simply put a dot at the center of a watermark bump in the image as shown in Figure 8 from which the ground truth bump locations can be easily extracted. The ground truth targets of the CNN model are then computed based on the annotated bump locations by Eq.(1).

## 4.2 Performance measures

Generally, the retrieval of watermark bits can be seen as a binary classification problem with two symmetric classes. However, since in our case value 0 bits correspond to no alteration of the carrier surface and are indistinguishable from the background, we treat the retrieval process as a binary detection test. Thus, as performance measures of the overall watermark retrieval method we report sensitivity  $TPR=TP/(TP+FN)$ , specificity  $SPC=TN/(TN+FP)$ , precision  $PPV=TP/(TP+FP)$  and negative predictive value  $NPV=TN/(TN+FN)$ , where TP and FN are the numbers of value 1 bits retrieved correctly and correspondingly incorrectly, while TN and FP are the numbers of value 0 bits retrieved correctly and correspondingly incorrectly.

## 4.3 Experimental Results

We report results from four tests.

1. A 5-fold cross-validation test on the 16 printed objects that were used for the development of the CNN-3DW.

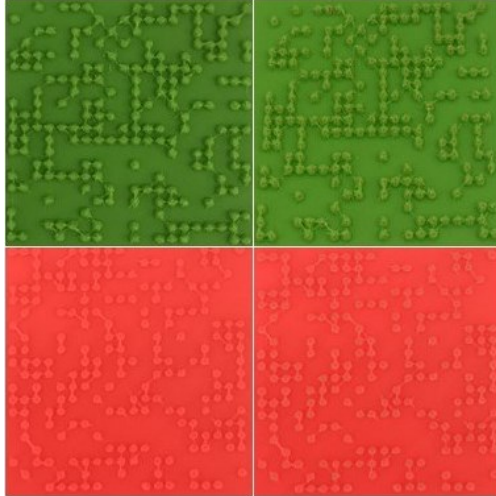


Figure 8: Two example of raw images (left) and annotated images (right) for ground truth bump location extraction.

2. A validation test on images from four objects printed after the development of the CNN-3DW was complete.
3. A cross-material validation test where training and test sets do not contain images of objects printed with the same material colour.
4. A test demonstrating the feasibility of an active learning approach, in which we identify a material colour on which the algorithm performs poorly, print more objects using that material and use their images to retrained the network.

#### 4.3.1 Experiment 1

In this experiment we assess the general accuracy of the method and how it is affected by material colour and illumination conditions. We use objects 1-16 which are printed using 9 material colours in total. From each object we capture 15 images of size  $3024 \times 4032$  with an iPhone 8 camera under different, arbitrary perspectives, 10 of them under natural light and 5 under extreme artificial illumination. From each object we select two natural and one artificial illumination image to create a test set containing 48 images in total, while the other 192 images used for training. We repeat this process 5 times, until all images have been used once for testing.

The results are summarized in Table 1. We can see that the proposed method performs well on most of the printed objects, dark green and transparent purple being the most notable exceptions. In contrast, a traditional image processing and analysis pipeline based on Local Binary Patterns and ellipse detection, which we developed for comparison purposes, did not generalize well. Figure 9 shows the LBPs from Wooden and Green material printouts. On the low background noise Wooden printout, they outperform CNNs with retrieval rates above 90%, however, on the high background noise Green material the traditional pipeline breaks down.

Notice that in this experiment we used only one transparent purple object, thus the poor material properties and not enough training data could explain the poor retrieval performance. In experiment 4 we employ a form of active learning [10] to study this further.

Table 2 shows average performances over all 16 printed objects for each illumination condition. As expected, extreme artificial light has a negative effect on performance.

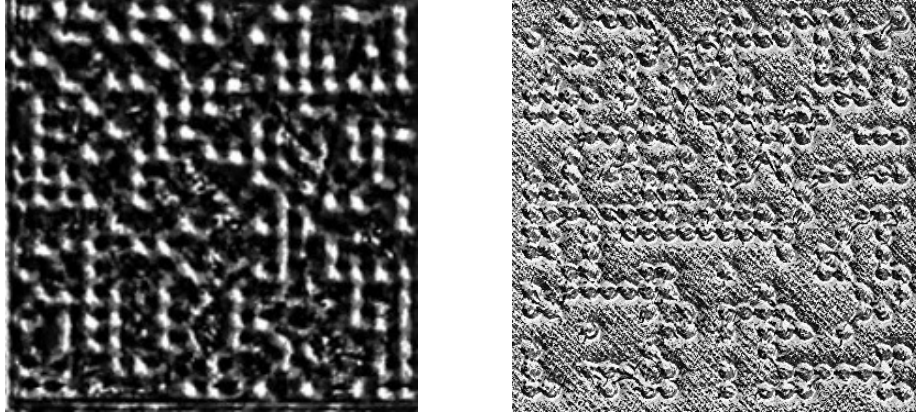


Figure 9: LBPs of the Wooden (left) and Green (right) material printouts.

### 4.3.2 Experiment 2

For this experiment we use images of objects 1-16 for training and test with images of objects 17-20. Notice that while in the previous experiment the watermark matrices of the test images also appear in the training set, with this test we can exclude the remote chance that CNN-3DW is memorizing parts of watermark matrices.

The results are shown in Table 3. Apart from averages we also report the results of an ensemble algorithm determining the value of each bit by a majority vote over the five images. Notice that the ensemble method is very much within the spirit of our target application scenario since modern mobile phones can easily capture and process short video sequences. The results show that CNN-3DW retrieval rates are independent if the watermark matrix and that majority vote can improve retrieval accuracy to levels that would be deemed satisfactory in a real life application.

### 4.3.3 Experiment 3

Here we use the same test set as in Experiment 2, but each of the four newly printed test objects is tested on a neural network trained only with images of different material colours. The aim of this test is to assess the generalisation ability of CNN-3DW on images from objects with unseen material colours.

The results are shown in Table 4. From the comparison between the results of Tables 3 and 4 we notice that CNN-3DW can handle some colours such as Blue and Dark Green quite well as unseen colours, while in some other cases (such as Wooden and Skin) the performance drops significantly.

### 4.3.4 Experiment 4

3D printed watermarking retrieval is an application well suited for the adoption of an active learning approach where we expand the training set with examples on which the current network underperforms and then we retrain. Indeed, on one hand, performance assessment of the ability of the algorithm to retrieve the correct bit values can be done completely automatically, on the other hand, the expansion of the training set requires the hand-annotation of images of watermarked objects, which is a laborious, tedious process. Therefore, being able to choose suitable images for inclusion to the training set is a matter of importance.

Table 1: Experiment 1: 5-fold cross validation.

	Colour	TPR	SPC	PPV	NPV
1	Green (a)	0.965	0.966	0.967	0.965
2	Green (b)	0.994	1	1	0.993
3	Dark Brown (a)	0.798	0.863	0.854	0.812
4	Dark Brown (b)	0.905	0.940	0.937	0.912
5	Blue (a)	0.964	0.998	0.998	0.966
6	Blue (b)	1	0.998	0.998	1
7	Dark Green (a)	0.662	0.698	0.699	0.661
8	Dark Green (b)	0.882	0.942	0.939	0.887
9	Wooden (a)	0.830	0.840	0.851	0.818
10	Wooden (b)	0.862	0.881	0.871	0.872
11	Luminous Red (a)	0.971	0.981	0.982	0.970
12	Luminous Red (b)	1	1	1	1
13	Skin (a)	1	1	1	1
14	Skin (b)	0.882	0.921	0.914	0.893
15	Bronze	0.889	0.901	0.900	0.890
16	Transparent Purple	0.542	0.862	0.756	0.685
		<b>0.895</b>	<b>0.897</b>	<b>0.895</b>	<b>0.885</b>

Table 2: Performance comparison under different illumination conditions.

	TPR	SPC	PPV	NPV
Natural light	0.89	0.93	0.92	0.89
Extreme artificial light	0.82	0.86	0.85	0.84

From Table 1 we notice that transparent purple is a particularly challenging material colour. We printed two more watermarked objects on this colour, capture 15 images from each object and added them to the training set. From Table 5 shows the performance of the algorithm, before and after retraining with the expanded set, on three the three transparent purple test images where it initially performed the worst. We notice a considerable performance improvement.

#### 4.3.5 Other experiments

The current retrieval algorithm works on planar only surface watermarks. An extension of the approach to other watermark carrier surfaces seems to be a problem akin to surface reconstruction, and rather orthogonal to the machine learning part of the algorithm on which this paper concentrates. To test this claim we printed similar watermarks on spherical surfaces and processed their images with CNN-3DW. In the examples shown in Figure 10 we notice that good quality confidence maps are indeed constructed.

In various watermarking applications the requirements for high retrieval accuracy are satisfied via the use of error correcting codes. In such cases, for obtaining optimal results, the choice of error correcting scheme could be informed by some knowledge of the distribution of the error. In an application scenario like ours, a natural question to ask is whether the position of a bit inside the  $20 \times 20$  information matrix, in particular its distance from the center of the matrix, correlates with the probability of correct retrieval. In a final test, on each of the 400 bit positions, we computed the accuracy rate over all 240 images of Experiment 1. We found a weak but not negligible correlation

Table 3: Test results on four post-development printed objects.

Colour	Metrics	TPR	SPC	PPV	NPV
Blue	Average	0.99	1.00	1.00	0.99
	Majority Vote	1.00	1.00	1.00	1.00
Wooden	Average	0.87	0.86	0.85	0.88
	Majority Vote	1.00	1.00	1.00	1.00
Dark	Average	0.81	0.85	0.84	0.82
Green	Majority Vote	0.98	1.00	1.00	0.98
Skin	Average	0.93	0.99	0.99	0.94
	Majority Vote	1.00	1.00	1.00	1.00

Table 4: Test results on objects printed with unseen material colours.

Colour	Metrics	TPR	SPC	PPV	NPV
Blue	Average	0.95	0.97	0.97	0.95
	Majority Vote	1.00	1.00	1.00	1.00
Wooden	Average	0.79	0.76	0.76	0.79
	Majority Vote	0.87	0.83	0.82	0.87
Dark	Average	0.74	0.82	0.80	0.76
Green	Majority Vote	0.91	0.94	0.94	0.91
Skin	Average	0.65	0.8	0.81	0.74
	Majority Vote	0.72	0.98	0.98	0.76

between accuracy rate and distance from the center of the information matrix with a Pearson coefficient of 0.46. That is, the further away from the center of the information matrix a bit is, the higher the probability to be correctly retrieved. While we do not have an intuitive explanation for this result, we notice that the algorithm performs better over the less congested parts of the watermark, that is, near the boundary and near the corners.

## 5 Conclusions and Future Work

We presented a method for retrieving digital information embedded as planar surface texture on a 3D printed object. The proposed method was tested extensively and it was shown to be a technically viable alternative to QR codes. Moreover, by integrating the information embedding process into the manufacturing process, we address several security vulnerabilities of the current widespread practice of displaying QR codes printed as separate items.

Table 5: An active learning approach on transparent purple objects.

Colour	Metrics	TPR	SPC	PPV	NPV
Image a	pre-active	0.48	0.68	0.58	0.59
	active	0.63	0.74	0.69	0.68
Image b	pre-active	0.69	0.75	0.72	0.72
	active	0.76	0.80	0.78	0.78
Image c	pre-active	0.58	0.64	0.60	0.62
	active	0.95	1.00	1.00	0.95

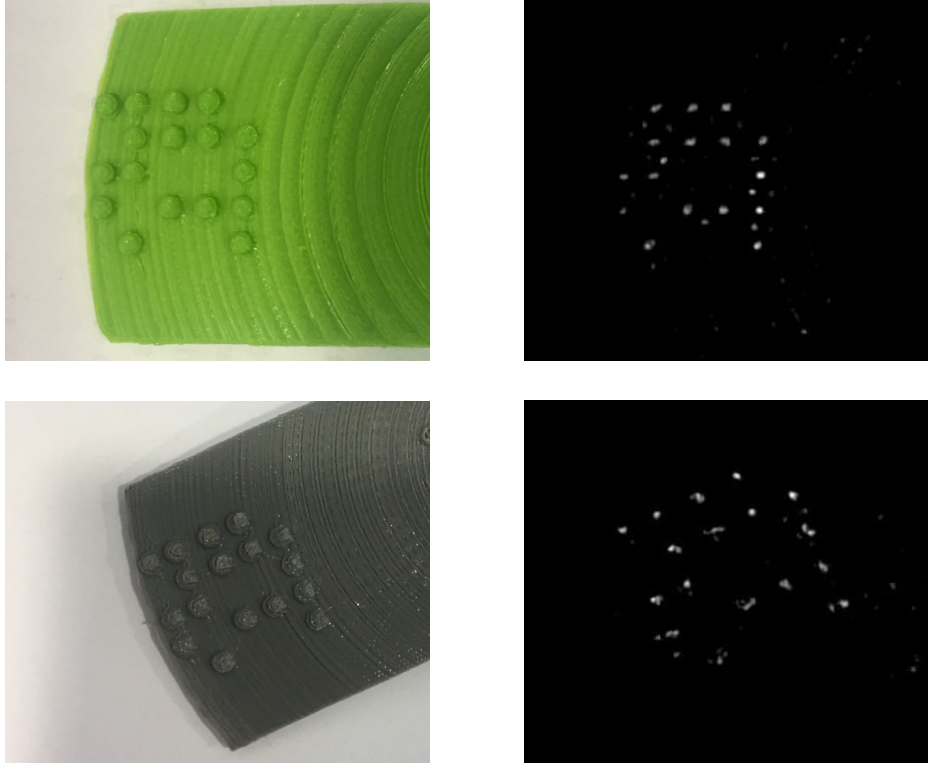


Figure 10: Confidence maps from non-planar watermarked surfaces.

## 5.1 Limitations and Future Work

In tailoring our algorithm we imposed various limitations to the solution, most of them aiming at isolating for study the machine learning part of the watermark extraction pipeline. Thus, the registration of the confidence map relies on the use of a second printing material of distinct colour to mark the corners of a square region of interest. Moreover, as a convenient robust solution to the watermark orientation problem, we use four distinct corner symbols consisting of one, two, three and four small dots, respectively. In another limitation, we restricted ourselves to planar surfaces. While CNN-3DW generates good quality confidence maps of non-planar watermarked surfaces, the extraction of the watermark from the confidence maps is essentially a surface reconstruction problem, quite different in nature from the bump detection part.

In the future, we plan to extend the current work into watermarks embedded on non-planar surfaces. As we discuss in Section 4, that extension shouldn't require any significant modifications of the CNN-3DW presented in this paper, but rather the development of new methods for processing the confidence maps. In another future research direction, we plan to develop higher capacity watermarks making use of more complex surface textures as carriers. In this case, we expect that the accurate retrieval of the watermark will require the development of more complex machine vision tools.

## References

- [1] Thompson, M.K., Moroni, G., Vaneker, T., Fadel, G., Campbell, R.I., Gibson, I., Bernard, A., Schulz, J., Graf, P., Ahuja, B., et al.: Design for additive manufacturing: Trends, opportun-

- ities, considerations, and constraints. *CIRP annals* **65** (2016) 737–760
- [2] Wong, K.V., Hernandez, A.: A review of additive manufacturing. *ISRN Mechanical Engineering* **2012** (2012)
  - [3] Terry, W.: Additive manufacturing and 3d printing state of the industry. Annual Worldwide Progress Report, Wohlers Associations (2012)
  - [4] Ohbuchi, R., Mukaiyama, A., Takahashi, S.: A frequency-domain approach to watermarking 3D shapes. *Computer Graphics Forum* **21** (2002) 373–382
  - [5] Bors, A.G.: Watermarking mesh-based representations of 3-d objects using local moments. *IEEE Transactions on Image processing* **15** (2006) 687–701
  - [6] Luo, M., Bors, A.G.: Surface-preserving robust watermarking of 3D shapes. *IEEE Trans. on Image Processing* **20** (2011) 2813–2826
  - [7] Yang, Y., Pintus, R., Rushmeier, H., Ivriissimtzis, I.: A 3d steganalytic algorithm and steganalysis-resistant watermarking. *IEEE transactions on visualization and computer graphics* **23** (2017) 1002–1013
  - [8] Macq, B., Alface, P.R., Montanola, M.: Applicability of watermarking for intellectual property rights protection in a 3D printing scenario. In: *Proc. of the International Conference on 3D Web Technology*, ACM (2015) 89–95
  - [9] Hou, J.U., Kim, D.G., Choi, S., Lee, H.K.: 3D Print-Scan Resilient Watermarking Using a Histogram-Based Circular Shift Coding Structure. In: *Proc. of the ACM Workshop on Information Hiding and Multimedia Security*. (2015) 115–121
  - [10] LeCun, Y., Bengio, Y., Hinton, G.: Deep learning. *nature* **521** (2015) 436
  - [11] LeCun, Y., Kavukcuoglu, K., Farabet, C., et al.: Convolutional networks and applications in vision. In: *ISCAS*. Volume 2010. (2010) 253–256
  - [12] Robert, C.: *Machine learning, a probabilistic perspective* (2014)
  - [13] Krizhevsky, A., Sutskever, I., Hinton, G.E.: Imagenet classification with deep convolutional neural networks. In: *Advances in neural information processing systems*. (2012) 1097–1105
  - [14] Simonyan, K., Zisserman, A.: Very deep convolutional networks for large-scale image recognition. *arXiv:1409.1556* (2014)
  - [15] Szegedy, C. et al.: Going deeper with convolutions. In: *IEEE CVPR*. (2015)
  - [16] Zhang, C., Li, H., Wang, X., Yang, X.: Cross-scene crowd counting via deep convolutional neural networks. In: *Proceedings of the IEEE Conference on Computer Vision and Pattern Recognition*. (2015) 833–841
  - [17] Zhang, Y., Zhou, D., Chen, S., Gao, S., Ma, Y.: Single-image crowd counting via multi-column convolutional neural network. In: *IEEE CVPR*. (2016) 589–597
  - [18] Mundhenk, T.N., Konjevod, G., Sakla, W.A., Boakye, K.: A large contextual dataset for classification, detection and counting of cars with deep learning. In: *European Conference on Computer Vision*, Springer (2016) 785–800

- [19] Ojala, T., Pietikäinen, M., Mäenpää, T.: Gray scale and rotation invariant texture classification with local binary patterns. In: ECCV, Springer (2000) 404–420
- [20] Zeiler M. et al.: On rectified linear units for speech processing. In: Acoustics, Speech and Signal Processing (ICASSP), IEEE (2013) 3517–3521
- [21] Chollet, F., et al.: Keras. <https://github.com/fchollet/keras> (2015)
- [22] Kingma, D.P., Ba, J.: Adam: A method for stochastic optimization. arXiv preprint arXiv:1412.6980 (2014)
- [23] Brown, L.G.: A survey of image registration techniques. ACM computing surveys (CSUR) **24** (1992) 325–376
- [24] Otsu, N.: A threshold selection method from gray-level histograms. IEEE transactions on systems, man, and cybernetics **9** (1979) 62–66